Omni-Effects: Unified and Spatially Control-Lable Visual Effects Generation

Fangyuan Mao 1*† Aiming Hao 1† Jintao Chen 1,2 Dongxia Liu 1,3 Xiaokun Feng 1,4 Jiashu Zhu 1 Meiqi Wu 1,4 Chubin Chen 1,3 Jiahong Wu 1‡ Xiangxiang Chu 1 AMAP, Alibaba Group 2 PKU 3 THU 4 CASIA

Project Page: https://amap-ml.github.io/Omni-Effects.github.io/



Figure 1: Capabilities for Diverse Customized Visual Effects. *Omni-Effects* supports both (a) single-VFX and (b) multi-VFX generation through pure prompt-guided generation. Integrated with the **Spatial-Aware Prompt**, *Omni-Effects* enables (c) precise spatial VFX control and (d) intricate object-based visual effects with targeted environmental transformations.

ABSTRACT

Visual effects (VFX) are essential visual enhancements fundamental to modern cinematic production. Although video generation models offer cost-efficient solutions for VFX production, current methods are constrained by per-effect LoRA training, which limits generation to single effects. This fundamental limitation impedes applications that require spatially controllable composite effects, i.e., the concurrent generation of multiple effects at designated locations. However, integrating diverse effects into a unified framework faces major challenges: interference from effect variations and spatial uncontrollability during multi-VFX joint training. To tackle these challenges, we propose *Omni-Effects*, a first unified framework capable of generating prompt-guided effects and spatially controllable composite effects. The core of our framework comprises two key innovations:

^{*}Work done during the internship at AMAP, Alibaba Group.

[†]Equal Contribution

[‡]Project Lead

(1) **LoRA-based Mixture of Experts (LoRA-MoE)**, which employs a group of expert LoRAs, integrating diverse effects within a unified model while effectively mitigating cross-task interference. (2) **Spatial-Aware Prompt (SAP)** incorporates spatial mask information into the text token, enabling precise spatial control. Furthermore, we introduce an Independent-Information Flow (IIF) module integrated within the SAP, isolating the control signals corresponding to individual effects to prevent any unwanted blending. To facilitate this research, we construct a comprehensive VFX dataset *Omni-VFX* via a novel data collection pipeline combining image editing and First-Last Frame-to-Video (FLF2V) synthesis, and introduce a dedicated VFX evaluation framework for validating model performance. Extensive experiments demonstrate that *Omni-Effects* achieves precise spatial control and diverse effect generation, enabling users to specify both the category and location of desired effects.

1 Introduction

Visual effects (VFX) play a crucial role in modern filmmaking, enabling the creation of immersive narratives and fantastical worlds. While traditional VFX pipelines, especially for composite effects requiring simultaneous coordination across different spatial locations, are notoriously complex and resource-intensive Chabanova (2022). Recent rapid advances in video generation technologies Yang et al. (2024); Bao et al. (2024); Kong et al. (2024); Wan et al. (2025) are driving a paradigm shift in VFX creation—transitioning from conventional methods to generative model-powered dynamic, efficient synthesis.

The inherent scarcity of VFX data and pronounced variability in dynamic characteristics across effects pose significant challenges to training generative models. Consequently, current methods Liu et al. (2025b) focus on single-effect generation, employing dedicated Low-Rank Adaptation (LoRA) Hu et al. (2022) tailored to individual effects. However, this paradigm struggles with multi-VFX scenes, exhibiting two critical limitations: Limitation 1. Cross-Adapter Interference where joint multi-LoRA activation Ding et al. (2023) induces spatial occlusion artifacts (Figure 2 (a)) and shared-subspace hybrid training triggers fidelity-degrading cross-effect confusion via task interference Zhang et al. (2025a) (Figure 2 (b, c)). Limitation 2. Spatial-Semantic Misalignment wherein the text-pixel space gap prevents precise spatial cue encoding for VFX placement (Figure 2 (d)).

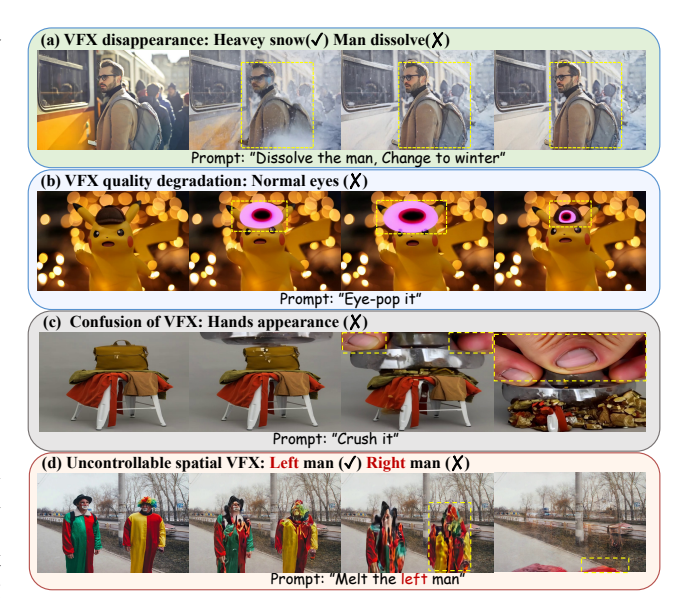


Figure 2: **Defects in standard video generation models.** (a) VFX disappearance, (b) quality degradation, (c) confusion between VFX elements, and (d) spatial uncontrollability.

These limitations fundamentally constrain conventional video generation adaptation to complex multiple VFX compositions (multi-VFX).

To address these limitations, we propose *Omni-Effects*, a unified framework modeling multi-VFX generation as a multi-condition video generation problem, where textual prompts specify effect categories while spatial masks define their precise locations. First, to tackle Limitation 1, we introduce a **LoRA-based Mixture of Experts (LoRA-MoE)** module Shazeer et al. (2017); Dou et al. (2023); Zhang et al. (2025c), which partitions effects into specialized subspaces, each optimized by dedicated expert branches, with a gating router dynamically activating relevant subspaces to minimize cross-task interference and enhance effect fidelity. Second, to overcome Limitation 2, we present

the **Spatial-Aware Prompt** (**SAP**), which integrates explicit mask-based spatial conditioning with textual inputs via full-attention mechanisms for accurate effect placement. To mitigate SAP cross-interference during concurrent application, we introduce the Independent-Information Flow (IIF) module, which isolates condition-specific information flows through IIF Attention Mask, preventing unintended effect blending. Collectively, these innovations enable *Omni-Effects*—to our knowledge, the first VFX framework—to achieve high-fidelity multi-VFX compositions with pixel-level spatial control. (Figure 1).

To advance this research, we construct a high-quality VFX dataset *Omni-VFX* and develop a specialized VFX data pipeline. This pipeline utilises image editing models Liu et al. (2025a) to generate source image pairs depicting initial/final effect states, which are then synthesised into VFX videos via the FLF2V framework (built on Wan2.1 Wan et al. (2025)). Rigorous manual filtering ensures quality while expanding coverage to 55 distinct effect categories. Further, we introduce an evaluation framework specifically designed for controllable VFX generation tasks. Comprehensive experiments validate the *Omni-Effects* framework's superior performance across three core capabilities: single-VFX, multi-VFX, and controllable VFX generation. In summary, the major contributions of our work are as follows:

- A unified VFX framework, *Omni-Effects*, is proposed to enable high-fidelity spatial controllable multi-VFX generation through a dual-core architecture: (1) **LoRA-MoE** modules unifying multi-VFX training, and (2) IIF-augmented **SAP** mechanisms enabling independent multi-condition control without interference.
- The most comprehensive VFX dataset *Omni-VFX* is developed with an automated production pipeline to support the generation of diverse high-quality VFX video, complemented by a comprehensive evaluation framework for rigorous controllable VFX assessment.
- Extensive experiments demonstrate that our *Omni-Effects* achieves precise spatial control
 and enables diverse VFX generation, thereby allowing users to specify both the category
 and location of desired effects.

2 RELATED WORKS

2.1 VIDEO GENERATION MODELS

Recent advances in diffusion-based video generation Chen et al. (2023); He et al. (2022); Zeng et al. (2024); Kong et al. (2024); Yang et al. (2024); HaCohen et al. (2024); Bao et al. (2024); Polyak et al. (2024); Wan et al. (2025); Teng et al. (2025); Seawead et al. (2025) have enabled text-to-video (T2V) and image-to-video (I2V) synthesis, where input images establish spatial context. As a critical I2V application, VFX generation creates unrealizable fantastical visuals. However, VFX data scarcity forces reliance on Low-Rank Adaptation (LoRA) Hu et al. (2022) for limited-data fine-tuning Liu et al. (2025b). This necessitates separate LoRA models per effect, while combined training causes performance degradation, fundamentally limiting multi-VFX generation within a single video.

Our architecture unifies multi-VFX training, avoids degradation, and enables concurrent multi-VFX generation.

2.2 CONDITIONAL VIDEO GENERATION

Condition-guided diffusion models leverage auxiliary inputs for precise output control, falling into two paradigms: spatial-fusion guidance and high-level semantic guidance. Spatial-fusion methods, exemplified by ControlNet Zhang et al. (2023), integrate condition inputs with denoising inputs. These methods Li et al. (2024); Bai et al. (2024); Bian et al. (2025); Xu et al. (2025b); Lei et al. (2025); Jiang et al. (2025) enable fine-grained spatial alignment while preserving the generation quality of pre-trained diffusion models. High-level semantic methods exploit latent interactions between conditions and the denoising process. Techniques include cross-attention based mechanisms Ye et al. (2023); Zhang et al. (2024); Zhou et al. (2025); Yuan et al. (2025) and conditional token concatenation strategies Wang et al. (2024); Huang et al. (2024b); Tan et al. (2025); Zhang et al. (2025b), dynamically modulate generation through semantic embeddings. Crucially, while these methods effectively handle individual conditions, they struggle to simultaneously and independently control multiple conditions, a critical requirement for professional VFX generation.

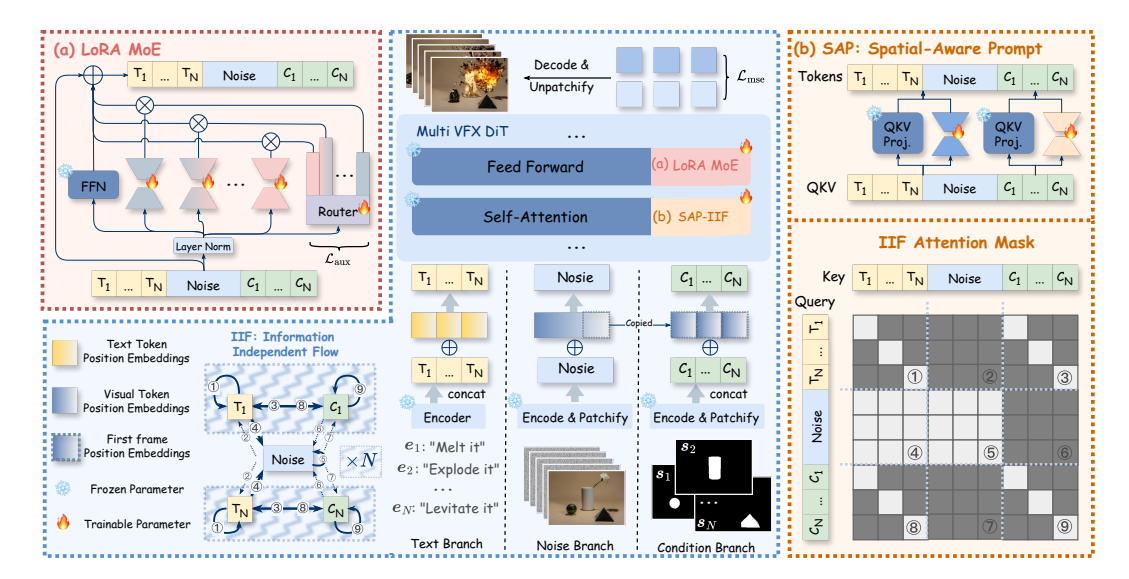


Figure 3: **Flowchart of proposed** *Omni-Effects*. Given a reference image and composite conditions of arbitrary length, *Omni-Effects* first encodes each input into corresponding tokens. These tokens are concatenated and processed sequentially through downstream DiT blocks. These blocks incorporate two key technologies: (a) **LoRA-MoE**, a MoE plugin replacing standard FFN linear layers to enable collaborative expert task-solving and (b) **SAP**, which fuses effect descriptors with spatial trigger information during the attention stage while mitigating cross-condition information leakage via an IIF mechanism. Note that, in the IIF, dashed lines represent blocked information flow, while solid lines indicate active information transmission.

Our model employs IIF-powered SAP control mechanisms to support independent, non-interfering control of multiple conditions within the same video.

3 Method

3.1 PRELIMINARIES

3.1.1 VIDEO DIFFUSION MODELS

Video generation models usually utilize the diffusion paradigm Ho et al. (2020); Lipman et al. (2022), which generates samples from a data distribution $p(x_0)$ by progressively denoising samples that are initially drawn from a Gaussian distribution $p(x_T)$. During training, clean samples $x_0 \sim p(x_0)$ undergo iterative corruption through T diffusion steps:

$$\boldsymbol{x}_{t} = \alpha_{t}\boldsymbol{x}_{0} + \sigma_{t}\boldsymbol{\epsilon}, \quad \boldsymbol{\epsilon} \sim \mathcal{N}\left(\boldsymbol{0}, \boldsymbol{I}\right), \ t = 1, ..., T$$
 (1)

where $\alpha_t, \sigma_t > 0$ are scalars that jointly define the Signal-to-Noise Ratio (SNR). The denoiser with parameter θ is optimized to predict the target noise ϵ . The optimization process is defined as:

$$\mathcal{L}_{\text{mse}}(\theta) = \mathbb{E}_{\boldsymbol{x}_{t},t,\boldsymbol{c},\boldsymbol{\epsilon}} \left[\left\| \boldsymbol{\epsilon} - \boldsymbol{\epsilon}_{\theta} \left(\boldsymbol{x}_{t},t,\tau \left(\boldsymbol{c} \right) \right) \right\|_{2}^{2} \right]$$
 (2)

where c is conditions (e.g., text and spatial location), and τ denotes the condition encoder. By replacing target noise ϵ with v, which is a weighted combination of x_0 and ϵ , as the prediction target, the v-prediction Salimans and Ho (2022) is derived, which is adopted in our *Omni-Effects* framework. Moreover, mainstream video generation leverages Diffusion Transformer (DiT) Peebles and Xie (2023); Ma et al. (2024); Chu et al. (2024) architecture by employing attention mechanisms to model spatiotemporal consistency while aligning conditional inputs with visual outputs Zheng et al. (2024). By integrating diffusion processes with Transformer architectures, the video generation performance is improved, leading to high-quality and accurate video synthesis results.

3.1.2 Spatially Controllable Multi-VFX Generation

In practical applications, it's often necessary to display different VFX at distinct locations throughout a video. We formalize this task as multi-conditional video generation, wherein video diffusion

models take a reference image and a set of N control signals $C = \{c_i\}_{i=1}^N$ as inputs. Each condition $c_i = (e_i, s_i)$ couples an effect descriptor e_i with a spatial trigger s_i , whereby the generated video x_0 applies effect e_i at the location specified by s_i . Specifically, we use a text prompt to describe the VFX, while using a spatial mask $m \in \mathbb{R}^{H \times W}$ to serve as the spatial trigger. A set of conditions is incorporated into the denoising process, and the denoiser prediction becomes:

$$\hat{\boldsymbol{v}} = \epsilon_{\theta} \left(\boldsymbol{x}_{t}, t, \left\{ \tau_{e}^{(i)} \left(\boldsymbol{e}_{i} \right) \right\}_{i=1}^{N}, \left\{ \tau_{s}^{(i)} \left(\boldsymbol{s}_{i} \right) \right\}_{i=1}^{N} \right), \tag{3}$$

where τ_e and τ_s denote the text and spatial mask encoder, respectively. Notice that, when N=1 and the spatial trigger is empty, the above task reduces to the traditional single-VFX generation task Liu et al. (2025b).

3.2 Omni-Effects

To model the above task, video diffusion models require simultaneous support for multi-VFX inference and spatial control capabilities. We accordingly propose *Omni-Effects*, building upon the CogVideoX Yang et al. (2024) architecture and incorporating two core components: **LoRA-MoE** and **Spatial-Aware Prompt**. The overview is illustrated in Figure 3, and the details are as follows.

3.2.1 LORA-MOE

As mentioned in Figure 2, both multi-LoRA parallel inference and single-LoRA unified training degrade performance. Crucially, we observe the synergistic mechanism in VFX training: compatible VFX-combination training enhances single-VFX generation quality (Figure 4). This discovery motivates our adaptive task-space partitioning strategy: inspired by MoE Shazeer et al. (2017) architectures, we partition distinct effects into specialized subspaces and deploy a gating router for adaptive subspace selection.

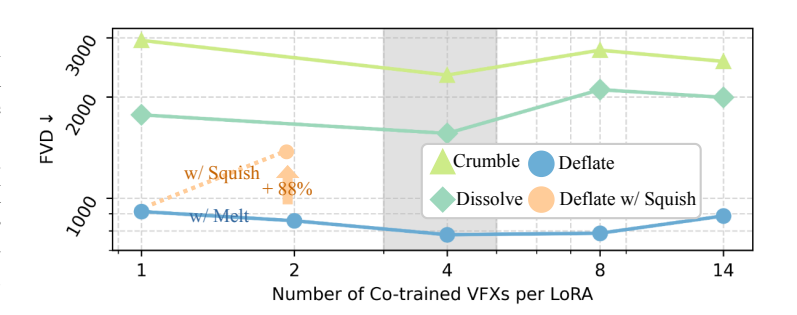


Figure 4: **FVD** scores for diverse VFX trained with a shared LoRA. VFX performance exhibits an initial improvement followed by progressive degradation with increasing numbers of co-trained effects. This indicates inherent effect clustering: synergistic groups (e.g., Melt-like effects) improve co-training performance, while incompatible combinations (e.g., Deflate + Squish) suffer from mode collapse and underperform relative to compatible sets. Note that, **lower FVD** values indicate superior performance, with optimal VFX results uniformly achieved when the number of co-trained VFX equals 4.

Specifically, LoRA-MoE Dou et al. (2023) integrates MoE with LoRA (Figure 3 (a)), which employs an expert ensemble where each LoRA specializes in distinct VFX manifolds. Formally, for input token $\boldsymbol{x} \in \mathbb{R}^d$, a weight is obtained by a gating network $G: \mathbb{R}^d \mapsto \mathbb{R}^n$ for each expert, resulting in $G(\boldsymbol{x}) = [G(\boldsymbol{x})_1, G(\boldsymbol{x})_2, ..., G(\boldsymbol{x})_n]$, where n represents the number of experts. Each expert E_i implements LoRA decomposition:

$$E_i(\mathbf{x}) = \frac{\alpha}{r} \mathbf{x} \mathbf{A}_i \mathbf{B}_i, \ \mathbf{A}_i \in \mathbb{R}^{d \times r}, \ \mathbf{B}_i \in \mathbb{R}^{r \times d},$$
(4)

where r denotes the low-rank and α is a scaling factor. The final prediction combines base model and expert outputs:

$$y = \text{Base}(x) + \sum_{i=1}^{n} G(x)_{i} \odot E_{i}(x),$$
 (5)

This MoE-structured plugin replaces standard FFN linear layers, enabling collaborative expert task-solving. During training, Top-k routing strategy ($k \le n$) is adopted to enforce exactly k non-zero entries in $G(\boldsymbol{x})$. At inference, all experts are activated to prevent effect suppression caused by Top-k

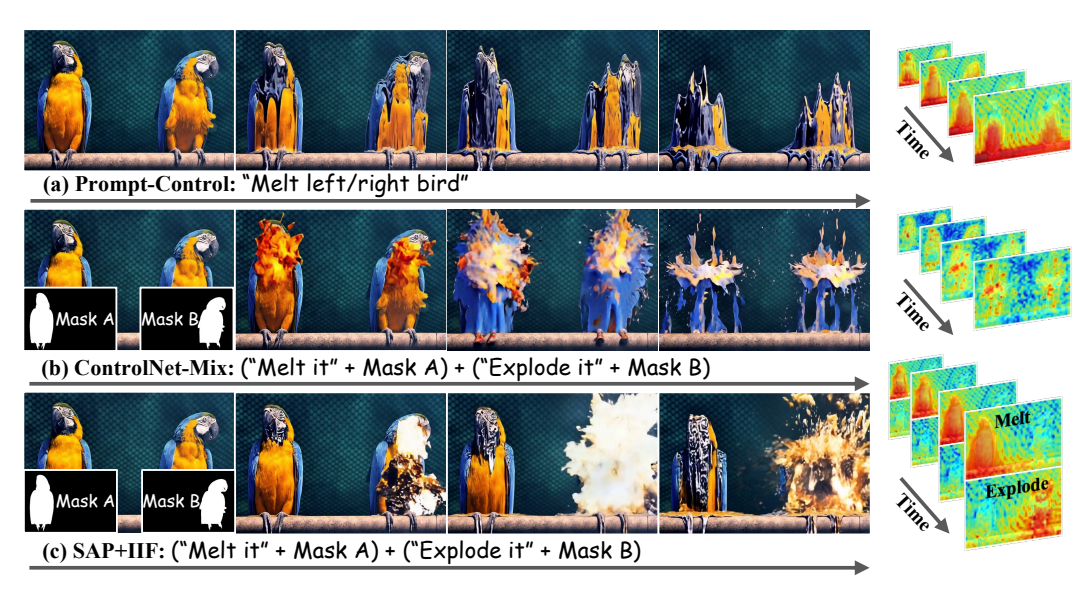


Figure 5: **Visualization of controllable VFX performance and attention maps.** (a) Position description lacks spatial control; (b) ControlNet faces inter-condition interference, leading to VFX leakage and artifacts; (c) Proposed **SAP+IIF** achieves precise positional controllability while preventing mutual interference between multi-VFX.

filtering, omitting critical experts, which is essential for multi-VFX combination generation. Moreover, to mitigate workload imbalance caused by the gating network favoring a few experts during training, we also employ a balanced routing auxiliary loss \mathcal{L}_{aux} Fedus et al. (2022). Comprehensive details are provided in Supplement A. The final training objective is expressed as: $\mathcal{L} = \mathcal{L}_{mse} + \beta \mathcal{L}_{aux}$, where β is hyperparameter.

3.2.2 SPATIAL-AWARE PROMPT

For condition $c_i = (e_i, s_i)$, embedding positional descriptors within text prompts proves insufficient for precise spatial control. To investigate this phenomenon, we visualize attention maps across diverse prompts. Crucially, attention consistently activates identical regions regardless of prompt semantics (Figure 5 (a)), evidencing textual position cues' failure to direct activation toward specified targets. Prior work Liu et al. (2025b); Jiang et al. (2025) mitigates this via ControlNet Zhang et al. (2023) to extract a mask sequence for generation guidance. However, this solution suffers from two critical limitations:

- 1. **Significant parameter overhead**: ControlNet duplicates a portion of the base model's parameters (typically half), requiring substantial extra trainable weights;
- 2. **Severe cross-condition interference**: During multi-VFX generation, parallel ControlNet inference suffers from information leakage, manifesting as erroneous co-occurrence of effect e_i and e_j at positions s_i and s_j respectively (Figure 5 (b)).

In summary, signals within composite conditions must be integrated while preventing cross-condition interference to ensure robust performance. We address these challenges by proposing the **Spatial-Aware Prompt** to directly inject spatial information into prompts tokens via enhanced spatial-text condition token interactions within attention mechanism, enabling controllable generation with minimal parameter/computational overhead. Building on this, we introduce Information-Independent Flow, which utilizes a designed attention mask to restrict cross-condition information exchange, thereby preventing interference between distinct control streams. Formally, given a set of conditions C, encoder processing yields text condition tokens $\left\{\tau_e^{(i)}\left(e_i\right)\right\}_{i=1}^N$ and spatial condition tokens $\left\{\tau_e^{(i)}\left(s_i\right)\right\}_{i=1}^N$, which are sequentially concatenated with the noisy latent x_t to form the inputs Q, K and V. Then we define an attention mask $M \in \{0, -\infty\}^{l \times l}$ (l is the total sequence length) to regulate attention flow (Figure 3 (b), details are in Supplement A) that blocks condition-to-

condition and noise-to-condition interactions, eliminating cross-condition leakage to prevent effect misalignment or blending. The final output of attention is expressed as:

$$y = \text{Softmax}\left(QK^T/\sqrt{d_k} + M\right)V,$$
 (6)

where d_k denotes the feature dimension. To enhance spatial conditioning alignment with noisy latents, we inject positional embeddings from x_t 's initial frame into $\tau_s^{(i)}(s_i)$, coupled with a dedicated Spatial-Condition LoRA. Crucially, all spatial conditions share identical LoRA parameters while maintaining a common base LoRA across other branches, ensuring efficient conditional injection without disrupting pretrained representations. Each text condition is individually processed through text encoder while sharing identical positional encoding. As shown in Figure 5 (c), our SAP+IIF achieves precise VFX targeting in target regions with non-overlapping activation zones.

4 Data and Training

4.1 Dataset Collection

VFX fundamentally manifest as radical spatio-temporal state transformations (e.g., explosion). Despite modern techniques like animation and Computer Graphics Interface (CGI) Chabanova (2022), modeling such dynamics remains challenging. We introduce a novel pipeline: for any input image, Step1X-Edit Liu et al. (2025a) produces its modified counterpart to establish boundary frames defining a VFX's initial and terminal states. This constraint provides strong transformation priors for generative models. The FLF2V framework Wan et al. (2025) then synthesizes the final video by compressing VFX production into boundary-constrained state-transition path search, significantly reducing modeling complexity. Through curated manual selection, we build a comprehensive dataset *Omni-VFX* spanning 55 distinct VFX across instantaneous environmental shifts, artistic styles, human emotions, and so on, enabling diverse creative applications. For more data details, please refer to Supplement B.

4.2 Training

Since our training dataset contains only single-VFX without multi-VFX data, empirical observations reveal that standard training fails to achieve controllable multi-VFX generation. We overcome this with a tri-level solution. At the **data** level, through random cropping and splicing with two videos, and random temporal freezing, we generate pseudo multi-VFX videos with corresponding masks. At the **scheduler** level, Non-Uniform Sampling prioritizes denoising steps $\in [900, 1000]$ (early stage) for spatial control learning with increased batch allocation, while dedicating fewer batches to detail refinement in lower steps $\in [0, 900]$, motivated by empirical findings that enhanced focus on early denoising accelerates model convergence. At the **training strategy** level, iterative single to multi-VFX (N=2) fine-tuning ensures stable convergence and performance gains. For more training details, please refer to Supplement $\bf C$.

5 EXPERIMENTS

5.1 EXPERIMENTAL SETUP

5.1.1 EVALUATION METRICS

Following previous work Liu et al. (2025b), for single-VFX evaluation, we employ two established metrics: Fréchet Video Distance (FVD) Unterthiner et al. (2018) for overall fidelity and Dynamic Degree Huang et al. (2024c) for motion dynamics. For controllable VFX, we introduce three novel metrics. *Regional Dynamic Degree* (RDD), which utilizes optical flow and masks, quantifies the strength of motion within the target region, thereby quantifies motion strength within target regions to measure visual impression. *Effect Occurrence Rate* (EOR), which is computed by inputting both the video and a given prompt template into Gemini2.5 Comanici et al. (2025) to obtain the answer, measures intended effect trigger frequency, indicating generation reliability. Building upon EOR, *Effect Controllability Rate* (ECR) assesses spatial precision by verifying VFX confinement to designated areas. Complete metric details appear in Supplement **D**.

Metrics	Methods	Cake-ify	Crumble	Crush	Decapitate	Deflate	Dissolve	Eye-pop	Harley	Inflate	Levitate	Melt	Squish	Ta-da	Venom	Avg.	Param.#
FVD↓	Single LoRA Mix LoRA	2138 1674	2947 2552	1496 1772	1190 1299	913 886	1770 1995	1995 1725	3576 4496	1505 2042	1401 1006	2827 2748	$\frac{1415}{1225}$	1053 1240	4146 3923	2026 2041	132.1M 9.4M
	LoRA-MoE	1506	1641	1213	1177	839	1118	1460	3330	1304	736	2512	1561	1064	3339	1628	28.5M
Dynamic Degree	Single LoRA Mix LoRA	0.8 0.8	0.8 0.8	0.0	0.6 0.6	0.0	0.8 0.8	0.0 0.0	1.0 1.0	0.8 0.8	0.0	0.6 0.6	1.0 1.0	1.0 1.0	1.0 1.0	0.60 0.60	132.1M 9.4M
	LoRA-MoE	1.0	1.0	0.6	0.6	0.0	0.4	0.0	1.0	1.0	0.0	0.6	1.0	1.0	1.0	0.66	28.5M

Table 1: **Performance comparison on OpenVFX dataset. Param.** # represents the average training parameters per effect. And the highest metric values are highlighted in **bold**, with the second-best underlined.

Methods		RD	D↑		EOR↑				ECR↑			
	Melt	Levitate	Explode	Avg.	Melt	Levitate	Explode	Avg.	Melt	Levitate	Explode	Avg.
CogVideoX	0.91	0.99	1.11	1.00	0.06	0.09	0.11	0.09	0.00	0.00	0.00	0.00
LTX-Video	0.12	0.11	0.14	0.12	0.05	0.02	0.05	0.04	0.00	0.00	0.00	0.00
Wan-2.1	2.06	1.57	2.38	2.00	0.11	0.02	0.03	0.05	0.02	0.00	0.00	0.01
CogV+CN	3.80	2.39	2.09	2.76	0.95	0.80	0.82	0.86	0.56	0.36	0.70	0.54
Ours	2.69	2.22	3.87	2.93	0.99	0.94	0.99	0.97	0.93	0.83	0.89	0.88

Table 2: **Quantitative Results of Single-VFX Control Generation.** We compare *Omni-Effects* with representative open-source video generation models under three controllable VFX scenarios: Melt, Levitate, and Explode.

5.1.2 IMPLEMENTATION DETAILS

Training employs a CogVideoX-5B backbone with LoRA rank of 128 with a total of n=8 experts, generating $49\times480\times720$ resolution videos. For loss, β is set to 0.01. We utilize 8 H20 GPUs (96GB) with a batch size of 1 per GPU. We use AdamW Loshchilov and Hutter (2017) at a constant 10^{-4} learning rate for 5,000 steps. During inference, DDIM Nichol and Dhariwal (2021) sampling (50 steps) with CFG Ho and Salimans (2022) scale 6.0 is applied, which can be perform on a single GPU. Extended details are in Supplement $\bf C$.

5.2 QUANTITATIVE RESULTS

In the following, we evaluate the effectiveness of *Omni-Effects* by comparing it with baseline models on unified and controllable VFX generation tasks.

5.2.1 Unified VFX Generation

We evaluate the LoRA-MoE against VFX-specific training LoRA and mix training LoRA for all VFX on the public OpenVFX dataset as detailed in Table 1. LoRA-MoE achieves the best performance across different types of VFX, while significantly reducing the number of trainable parameters. This demonstrates the effectiveness of the designed VFX task-subspace partitioning strategy. Qualitative results are shown in Supplement $\bf E$.

5.2.2 CONTROLLABLE VFX GENERATION

To evaluate our model, we perform comprehensive experiments for single- and multi-VFX control, comparing with state-of-the-art methods including (a) CogVideoX Yang et al. (2024), (b) LTX-Video HaCohen et al. (2024), (c) Wan2.1 Wan et al. (2025), and (d) CogVideoX integrated with ControlNet (CogV+CN). Evaluation targets three spatially localized VFX types—Explode, Melt, and Levitate—to ensure contamination-free assessment.

Single-VFX Control. Table 2 demonstrates baseline methods' fundamental limitations in synthesizing target VFX and achieving precise spatial control. While CogV+CN can synthesize VFX, it exhibits limited controllability. In comparison, *Omni-Effects* achieves the best performance with **0.97** EOR and **0.88** ECR, significantly outperforming all baselines in both generation quality and spatial control precision. This validates that our proposed SAP effectively integrates VFX descrip-

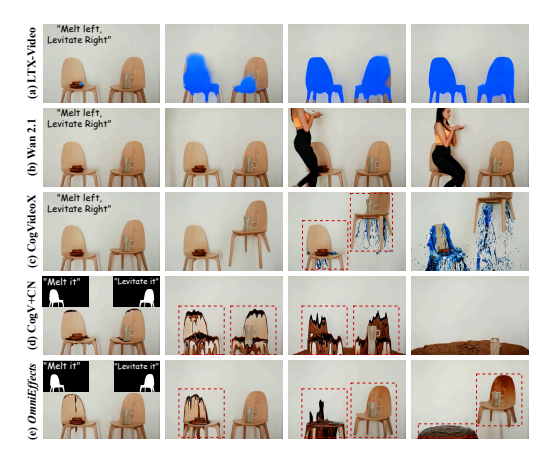


Figure 6: Qualitative Comparison of Multi-VFX Generation. The desired outcome requires the left chair to melt while the right levitates simultaneously.



Figure 7: **Effect of Different Attention Masks** in **SAP**. Attention Masks are progressively removed while information flow constraints are relaxed from top to bottom.







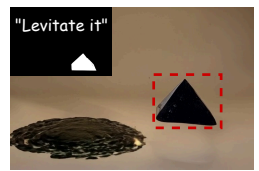


Figure 8: **Scalable VFX augmentation.** *Omni-Effects* supports inference-time extension to diverse VFX composition.

tors with spatial triggers without introducing substantial additional training parameters. Qualitative comparisons are shown in Supplement E.

Multi-VFX Control. For multi-VFX generation using two effects combinations, Table 3 shows baseline models consistently failing to generate or spatially control VFX. *Omni-Effects* achieves precise spatial control over simultaneous VFX. Moreover, Figure 6 demonstrates *Omni-Effects*' superiority: when instructed to melt the left chair while levitating the right chair, CogVideoX erroneously applies melting to both

Methods	Me	lt+Levi	tate	Melt+Explode				
11100110015	RDD↑	EOR↑	ECR ↑	RDD↑	EOR↑	ECR ↑		
CogVideoX	1.80	0.00	0.00	0.96	0.03	0.00		
LTX-Video	0.11	0.00	0.00	0.13	0.00	0.00		
Wan-2.1	1.93	0.01	0.00	3.10	0.01	0.00		
CogV+CN	3.18	0.09	0.05	<u>3.60</u>	0.08	0.08		
Ours	2.63	0.68	0.41	4.59	0.62	0.50		

Table 3: Quantitative Results of Multi-VFX Generation.

objects; CogV+CN correctly renders melting but fails to generate levitation; whereas *Omni-Effects* simultaneously executes both VFX through spatial condition. This performance validates our proposed IIF's efficacy in mitigating cross-condition interference. The user study is shown in Supplement **E**.

5.2.3 GENERALIZATION

Despite being trained with only N=2 effects, our model generalizes to diverse mask conditions during inference using the shared Spatial-Condition LoRA, thereby extending to the generation of more concurrent control VFX (N>2). *Omni-Effects* demonstrates robust extensibility, successfully handling complex effect combinations (Figures 1 (d) and 8), validating its test-time scalable VFX control capability.

5.3 ABLATION STUDIES

5.3.1 LORA-MOE

Ablation study on expert count n and Top-k selection (Table 4) reveals that scaling experts improves generation quality at increased parameter cost. Crucially, our MoE architecture with minimal experts surpasses LoRA baselines (Table 1), demonstrating efficient VFX adaptation through parameter-optimized expert aggregation.

Metrics	Model	Avg.	Param.#
FVD↓	4 Experts+Top1	1762	18.9
	8 Experts+Top2	1628	28.5
Dynamic Degree	4 Experts+Top1	0.65	18.9
	8 Experts+Top2	0.66	28.5

Table 4: Ablation study on LoRA MoE settings.

5.3.2 SAP+IIF

Ablation study on SAP+IIF reveal critical insights in attention mechanisms corresponding to information flow. Removing SAP attention masks from regions $\{@, @, @\}$ causes melting artifacts on levitating objects (Figure 7 (b, c)), exposing information leakage, while complete attention induces uncontrolled object melting, demonstrating excessive information interaction degrades control. Strategic masking of $\{@, @, @\}$ prevents leakage while preserving independent information flow in target regions. Additional ablation studies are detailed in the Supplement \mathbf{F} .

6 Conclusion

In this paper, we propose *Omni-Effects*, a unified framework for generating customized VFX videos. It supports the creation of diverse VFX, ranging from single-VFX, multi-VFX to spatially controllable multi-VFX. To achieve these, our framework integrates two core modules: LoRA-MoE and SAP-IIF. Specifically, the LoRA-MoE module mitigates cross-condition interference arising during mix training of multi-VFX. The SAP module, on the other hand, fuses VFX descriptors with spatial trigger information and tackles cross-condition information leakage via an IIF mechanism. Through the synergistic integration of LoRA-MoE and SAP-IIF, Omni-Effects enables precise spatial control and produces high-fidelity multi-VFX composites. We also develop a comprehensive VFX dataset Omni-VFX with a specialized data production pipeline and an evaluation framework tailored for controllable VFX generation to further validate our approach. Extensive experiments demonstrate the robustness of Omni-Effects across complex, multi-condition VFX generation scenarios. Multi-VFX generation represents a domain of substantial practical value coupled with persistent technical challenges. To the best of our knowledge, this work pioneers the first comprehensive framework explicitly addressing this complex problem. Our methodology substantively advances controllable multi-VFX synthesis capabilities while unlocking novel applications across film production, game development, and advertising creatives.

REFERENCES

Jianhong Bai, Menghan Xia, Xintao Wang, Ziyang Yuan, Xiao Fu, Zuozhu Liu, Haoji Hu, Pengfei Wan, and Di Zhang. Syncammaster: Synchronizing multi-camera video generation from diverse viewpoints. arXiv preprint arXiv:2412.07760, 2024.

Jinze Bai, Shuai Bai, et al. Qwen technical report. arXiv preprint arXiv:2309.16609, 2023.

Fan Bao, Chendong Xiang, Gang Yue, Guande He, Hongzhou Zhu, Kaiwen Zheng, Min Zhao, Shilong Liu, Yaole Wang, and Jun Zhu. Vidu: a highly consistent, dynamic and skilled text-to-video generator with diffusion models. *arXiv preprint arXiv:2405.04233*, 2024.

Yuxuan Bian, Zhaoyang Zhang, Xuan Ju, Mingdeng Cao, Liangbin Xie, Ying Shan, and Qiang Xu. Videopainter: Any-length video inpainting and editing with plug-and-play context control. In *Proceedings of the Special Interest Group on Computer Graphics and Interactive Techniques Conference Conference Papers*, pages 1–12, 2025.

Anastasia Chabanova. VFX-A new frontier: The impact of innovative technology on visual effects. PhD thesis, University of Westminster, 2022.

- Haoxin Chen, Menghan Xia, Yingqing He, Yong Zhang, Xiaodong Cun, Shaoshu Yang, Jinbo Xing, Yaofang Liu, Qifeng Chen, Xintao Wang, et al. Videocrafter1: Open diffusion models for high-quality video generation. *arXiv preprint arXiv:2310.19512*, 2023.
- Rui Chen, Lei Sun, Jing Tang, Geng Li, and Xiangxiang Chu. Finger: Content aware fine-grained evaluation with reasoning for ai-generated videos. In *ACM MM*, 2025.
- Xiangxiang Chu, Jianlin Su, Bo Zhang, and Chunhua Shen. Visionllama: A unified llama backbone for vision tasks. In ECCV, 2024.
- Xiangxiang Chu, Renda Li, and Yong Wang. Usp: Unified self-supervised pretraining for image generation and understanding. In *ICCV*, 2025.
- Gheorghe Comanici, Eric Bieber, Mike Schaekermann, Ice Pasupat, Noveen Sachdeva, Inderjit Dhillon, Marcel Blistein, Ori Ram, Dan Zhang, Evan Rosen, et al. Gemini 2.5: Pushing the frontier with advanced reasoning, multimodality, long context, and next generation agentic capabilities. arXiv preprint arXiv:2507.06261, 2025.
- Ning Ding, Yujia Qin, Guang Yang, Fuchao Wei, Zonghan Yang, Yusheng Su, Shengding Hu, Yulin Chen, Chi-Min Chan, Weize Chen, et al. Parameter-efficient fine-tuning of large-scale pre-trained language models. *Nature machine intelligence*, 5(3):220–235, 2023.
- Shihan Dou, Enyu Zhou, Yan Liu, Songyang Gao, Jun Zhao, Wei Shen, Yuhao Zhou, Zhiheng Xi, Xiao Wang, Xiaoran Fan, et al. Loramoe: Alleviate world knowledge forgetting in large language models via moe-style plugin. arXiv preprint arXiv:2312.09979, 2023.
- William Fedus, Barret Zoph, and Noam Shazeer. Switch transformers: Scaling to trillion parameter models with simple and efficient sparsity. *Journal of Machine Learning Research*, 23(120):1–39, 2022.
- Xiaokun Feng, Haiming Yu, Meiqi Wu, Shiyu Hu, Jintao Chen, Chen Zhu, Jiahong Wu, Xiangxiang Chu, and Kaiqi Huang. Narrlv: Towards a comprehensive narrative-centric evaluation for long video generation models. *arXiv preprint arXiv:2507.11245*, 2025.
- Yoav HaCohen, Nisan Chiprut, Benny Brazowski, Daniel Shalem, Dudu Moshe, Eitan Richardson, Eran Levin, Guy Shiran, Nir Zabari, Ori Gordon, et al. Ltx-video: Realtime video latent diffusion. arXiv preprint arXiv:2501.00103, 2024.
- Yingqing He, Tianyu Yang, Yong Zhang, Ying Shan, and Qifeng Chen. Latent video diffusion models for high-fidelity long video generation. *arXiv* preprint arXiv:2211.13221, 2022.
- Jonathan Ho and Tim Salimans. Classifier-free diffusion guidance. arXiv preprint arXiv:2207.12598, 2022.
- Jonathan Ho, Ajay Jain, and Pieter Abbeel. Denoising diffusion probabilistic models. *Advances in neural information processing systems*, 33:6840–6851, 2020.
- Edward J Hu, Yelong Shen, Phillip Wallis, Zeyuan Allen-Zhu, Yuanzhi Li, Shean Wang, Lu Wang, Weizhu Chen, et al. Lora: Low-rank adaptation of large language models. *ICLR*, 1(2):3, 2022.
- Hailang Huang, Yong Wang, Zixuan Huang, Huaqiu Li, Tongwen Huang, Xiangxiang Chu, and Richong Zhang. Mmgenbench: Fully automatically evaluating lmms from the text-to-image generation perspective. arXiv preprint arXiv:2411.14062, 2024a.
- Lianghua Huang, Wei Wang, Zhi-Fan Wu, Yupeng Shi, Huanzhang Dou, Chen Liang, Yutong Feng, Yu Liu, and Jingren Zhou. In-context lora for diffusion transformers. *arXiv preprint arXiv:2410.23775*, 2024b.
- Ziqi Huang, Yinan He, Jiashuo Yu, Fan Zhang, Chenyang Si, Yuming Jiang, Yuanhan Zhang, Tianxing Wu, Qingyang Jin, Nattapol Chanpaisit, et al. Vbench: Comprehensive benchmark suite for video generative models. In *Proceedings of the IEEE/CVF Conference on Computer Vision and Pattern Recognition*, pages 21807–21818, 2024c.
- Zeyinzi Jiang, Zhen Han, Chaojie Mao, Jingfeng Zhang, Yulin Pan, and Yu Liu. Vace: All-in-one video creation and editing. arXiv preprint arXiv:2503.07598, 2025.
- Weijie Kong, Qi Tian, Zijian Zhang, Rox Min, Zuozhuo Dai, Jin Zhou, Jiangfeng Xiong, Xin Li, Bo Wu, Jianwei Zhang, et al. Hunyuanvideo: A systematic framework for large video generative models. arXiv preprint arXiv:2412.03603, 2024.
- Rui Lan, Yancheng Bai, Xu Duan, Mingxing Li, Dongyang Jin, Ryan Xu, Lei Sun, and Xiangxiang Chu. Flux-text: A simple and advanced diffusion transformer baseline for scene text editing. arXiv preprint arXiv:2505.03329, 2025.

- Guojun Lei, Chi Wang, Rong Zhang, Yikai Wang, Hong Li, and Weiwei Xu. Animateanything: Consistent and controllable animation for video generation. In *Proceedings of the Computer Vision and Pattern Recognition Conference*, pages 27946–27956, 2025.
- Ming Li, Taojiannan Yang, Huafeng Kuang, Jie Wu, Zhaoning Wang, Xuefeng Xiao, and Chen Chen. ControlNet++: Improving conditional controls with efficient consistency feedback. In *European Conference on Computer Vision*, pages 129–147. Springer, 2024.
- Xinran Ling, Chen Zhu, Meiqi Wu, Hangyu Li, Xiaokun Feng, Cundian Yang, Aiming Hao, Jiashu Zhu, Jiahong Wu, and Xiangxiang Chu. Vmbench: A benchmark for perception-aligned video motion generation. In *ICCV*, 2025.
- Yaron Lipman, Ricky TQ Chen, Heli Ben-Hamu, Maximilian Nickel, and Matt Le. Flow matching for generative modeling. *arXiv preprint arXiv:2210.02747*, 2022.
- Shiyu Liu, Yucheng Han, Peng Xing, Fukun Yin, Rui Wang, Wei Cheng, Jiaqi Liao, Yingming Wang, Honghao Fu, Chunrui Han, et al. Step1x-edit: A practical framework for general image editing. *arXiv preprint arXiv:2504.17761*, 2025a.
- Xinyu Liu, Ailing Zeng, Wei Xue, Harry Yang, Wenhan Luo, Qifeng Liu, and Yike Guo. Vfx creator: Animated visual effect generation with controllable diffusion transformer. *arXiv preprint arXiv:2502.05979*, 2025b.
- Ilya Loshchilov and Frank Hutter. Decoupled weight decay regularization. arXiv preprint arXiv:1711.05101, 2017.
- Nanye Ma, Mark Goldstein, Michael S Albergo, Nicholas M Boffi, Eric Vanden-Eijnden, and Saining Xie. Sit: Exploring flow and diffusion-based generative models with scalable interpolant transformers. In *European Conference on Computer Vision*, pages 23–40. Springer, 2024.
- Alexander Quinn Nichol and Prafulla Dhariwal. Improved denoising diffusion probabilistic models. In *International conference on machine learning*, pages 8162–8171. PMLR, 2021.
- William Peebles and Saining Xie. Scalable diffusion models with transformers. In *Proceedings of the IEEE/CVF international conference on computer vision*, pages 4195–4205, 2023.
- Adam Polyak, Amit Zohar, Andrew Brown, Andros Tjandra, Animesh Sinha, Ann Lee, Apoorv Vyas, Bowen Shi, Chih-Yao Ma, Ching-Yao Chuang, et al. Movie gen: A cast of media foundation models. arXiv preprint arXiv:2410.13720, 2024.
- Tim Salimans and Jonathan Ho. Progressive distillation for fast sampling of diffusion models. *arXiv* preprint *arXiv*:2202.00512, 2022.
- Team Seawead, Ceyuan Yang, Zhijie Lin, Yang Zhao, Shanchuan Lin, Zhibei Ma, Haoyuan Guo, Hao Chen, Lu Qi, Sen Wang, et al. Seaweed-7b: Cost-effective training of video generation foundation model. *arXiv* preprint arXiv:2504.08685, 2025.
- Noam Shazeer, Azalia Mirhoseini, Krzysztof Maziarz, Andy Davis, Quoc Le, Geoffrey Hinton, and Jeff Dean. Outrageously large neural networks: The sparsely-gated mixture-of-experts layer. *arXiv preprint arXiv:1701.06538*, 2017.
- Zhenxiong Tan, Songhua Liu, Xingyi Yang, Qiaochu Xue, and Xinchao Wang. Ominicontrol: Minimal and universal control for diffusion transformer. In *Proceedings of the IEEE/CVF International Conference on Computer Vision*, pages 14940–14950, 2025.
- Zachary Teed and Jia Deng. Raft: Recurrent all-pairs field transforms for optical flow. In *European conference on computer vision*, pages 402–419. Springer, 2020.
- Hansi Teng, Hongyu Jia, Lei Sun, Lingzhi Li, Maolin Li, Mingqiu Tang, Shuai Han, Tianning Zhang, WQ Zhang, Weifeng Luo, et al. Magi-1: Autoregressive video generation at scale. arXiv preprint arXiv:2505.13211, 2025.
- Thomas Unterthiner, Sjoerd Van Steenkiste, Karol Kurach, Raphael Marinier, Marcin Michalski, and Sylvain Gelly. Towards accurate generative models of video: A new metric & challenges. *arXiv preprint arXiv:1812.01717*, 2018.
- Team Wan, Ang Wang, et al. Wan: Open and advanced large-scale video generative models. arXiv preprint arXiv:2503.20314, 2025.

- Jiawei Wang, Yuchen Zhang, Jiaxin Zou, Yan Zeng, Guoqiang Wei, Liping Yuan, and Hang Li. Boximator: Generating rich and controllable motions for video synthesis. *arXiv* preprint arXiv:2402.01566, 2024.
- Ryan Xu, Dongyang Jin, Yancheng Bai, Rui Lan, Xu Duan, Lei Sun, and Xiangxiang Chu. Scalar: Scale-wise controllable visual autoregressive learning. *arXiv preprint arXiv:2507.19946*, 2025a.
- Zunnan Xu, Zhentao Yu, Zixiang Zhou, Jun Zhou, Xiaoyu Jin, Fa-Ting Hong, Xiaozhong Ji, Junwei Zhu, Chengfei Cai, Shiyu Tang, et al. Hunyuanportrait: Implicit condition control for enhanced portrait animation. In Proceedings of the Computer Vision and Pattern Recognition Conference, pages 15909–15919, 2025b.
- Zhuoyi Yang, Jiayan Teng, Wendi Zheng, Ming Ding, Shiyu Huang, Jiazheng Xu, Yuanming Yang, Wenyi Hong, Xiaohan Zhang, Guanyu Feng, Da Yin, Xiaotao Gu, Yuxuan Zhang, Weihan Wang, Yean Cheng, Ting Liu, Bin Xu, Yuxiao Dong, and Jie Tang. Cogvideox: Text-to-video diffusion models with an expert transformer. *ArXiv*, abs/2408.06072, 2024.
- Hu Ye, Jun Zhang, Sibo Liu, Xiao Han, and Wei Yang. Ip-adapter: Text compatible image prompt adapter for text-to-image diffusion models. *arXiv* preprint arXiv:2308.06721, 2023.
- Shenghai Yuan, Jinfa Huang, Xianyi He, Yunyang Ge, Yujun Shi, Liuhan Chen, Jiebo Luo, and Li Yuan. Identity-preserving text-to-video generation by frequency decomposition. In *Proceedings of the Computer Vision and Pattern Recognition Conference*, pages 12978–12988, 2025.
- Yan Zeng, Guoqiang Wei, Jiani Zheng, Jiaxin Zou, Yang Wei, Yuchen Zhang, and Hang Li. Make pixels dance: High-dynamic video generation. In Proceedings of the IEEE/CVF Conference on Computer Vision and Pattern Recognition, pages 8850–8860, 2024.
- Juzheng Zhang, Jiacheng You, Ashwinee Panda, and Tom Goldstein. Lori: Reducing cross-task interference in multi-task low-rank adaptation. *arXiv* preprint arXiv:2504.07448, 2025a.
- Lvmin Zhang, Anyi Rao, and Maneesh Agrawala. Adding conditional control to text-to-image diffusion models. 2023 IEEE/CVF International Conference on Computer Vision (ICCV), pages 3813–3824, 2023.
- Yuxuan Zhang, Yiren Song, Jiaming Liu, Rui Wang, Jinpeng Yu, Hao Tang, Huaxia Li, Xu Tang, Yao Hu, Han Pan, et al. Ssr-encoder: Encoding selective subject representation for subject-driven generation. In *Proceedings of the IEEE/CVF Conference on Computer Vision and Pattern Recognition*, pages 8069–8078, 2024.
- Yuxuan Zhang, Yirui Yuan, Yiren Song, Haofan Wang, and Jiaming Liu. Easycontrol: Adding efficient and flexible control for diffusion transformer. In Proceedings of the IEEE/CVF International Conference on Computer Vision, pages 19513–19524, 2025b.
- Zechuan Zhang, Ji Xie, Yu Lu, Zongxin Yang, and Yi Yang. In-context edit: Enabling instructional image editing with in-context generation in large scale diffusion transformer. *arXiv preprint arXiv:2504.20690*, 2025c.
- Zangwei Zheng, Xiangyu Peng, Tianji Yang, Chenhui Shen, Shenggui Li, Hongxin Liu, Yukun Zhou, Tianyi Li, and Yang You. Open-sora: Democratizing efficient video production for all. *arXiv preprint arXiv:2412.20404*, 2024.
- Yujie Zhou, Jiazi Bu, Pengyang Ling, Pan Zhang, Tong Wu, Qidong Huang, Jinsong Li, Xiaoyi Dong, Yuhang Zang, Yuhang Cao, et al. Light-a-video: Training-free video relighting via progressive light fusion. arXiv preprint arXiv:2502.08590, 2025.

A METHOD

A.1 BALANCED ROUTING AUXILIARY LOSS \mathcal{L}_{AUX}

Drawing inspiration from Switch Transformers Fedus et al. (2022), we integrate a balanced routing auxiliary loss \mathcal{L}_{aux} into LoRA MoE training. Specifically, for a batch \mathcal{B} with \mathcal{T} tokens, define f_i as the fraction of tokens routed to expert i:

$$f_{i} = \frac{1}{\mathcal{T}} \sum_{\boldsymbol{x} \in \mathcal{B}} \mathbb{I} \left\{ \arg \max p\left(\boldsymbol{x}\right) = i \right\}, \tag{7}$$

and P_i is the mean router probability for expert i

$$P_{i} = \frac{1}{\mathcal{T}} \sum_{\boldsymbol{x} \in \mathcal{B}} p_{i}(\boldsymbol{x}). \tag{8}$$

The auxiliary loss encourages load balancing through:

$$\mathcal{L}_{\text{aux}} = n \sum_{i=1}^{n} f_i \cdot P_i, \tag{9}$$

which reaches its theoretical minimum of 1 when $p_i(\boldsymbol{x}) = 1/n$ uniformly $(\forall \boldsymbol{x}, i)$. When the gating network outputs an average probability distribution of $[1/n, \cdots, 1/n]$ for tokens in a batch, \mathcal{L}_{aux} achieves its minimum value as $n \sum_{i=1}^n 1/n \cdot 1/n = 1$

A.2 IIF ATTENTION MASK

The IIF Attention Mask is partitioned into two primary components:

- Condition Interaction: Within each condition pair c_i , comprising text $(\tau_e^{(i)}(e_i))$ and spatial condition $(\tau_s^{(i)}(s_i))$ tokens, tokens attend to each other. However, tokens within one condition pair are masked from all tokens in other condition pairs and from the noisy latent token x_t to prevent information leakage.
- Information Aggregation: The noisy latent token x_t attends to all text tokens $(\left\{\tau_e^{(k)}\left(e_k\right)\right\}_{k=1}^N)$ and to itself. This aggregates textual information for updating its representation. Crucially, x_t is masked from all spatial condition tokens $(\left\{\tau_s^{(k)}\left(s_k\right)\right\}_{k=1}^N)$, preventing direct access and avoiding redundancy.

Formally, the IIF Attention Mask M_{ij} for tokens x_i and x_j is defined as:

$$M_{ij} = \begin{cases} 0, & \text{if } x_i \text{ and } x_j \text{ belong to the same condition } \mathbf{c}_k \\ 0, & \text{if } x_i \in \mathbf{x}_t \text{ and } x_j \in \mathbf{x}_t \cup \left\{ \tau_e^{(k)} \left(\mathbf{e}_k \right) \right\}_{k=1}^N \\ -\infty, & \text{otherwise} \end{cases}$$
 (10)

B DATASET

B.1 DATASET COLLECTION

To augment our dataset, we employ three strategies: a novel **first-last frame generation** method and integrating external datasets.

Our dataset construction pipeline, outlined in Figure 9, follows a multi-stage generative approach. **Firstly**, we define target VFX categories spanning diverse styles (e.g., seasonal transformations, claymation, 3D doll rendering). An initial semantic analysis using Qwen Bai et al. (2023) classifies input images by content and style. **Secondly**, for each category, Step1X-Edit Liu et al. (2025a) generates stylistically consistent frame pairs (initial-final) conditioned on dynamically constructed prompts. These pairs are then analyzed by Qwen to produce descriptive text prompts, which undergo iterative refinement through Wan2.1-14B's Video Prompt Extender Wan et al. (2025) for temporal coherence. **Thirdly**, the optimized prompts and frames jointly drive Wan2.1-14B to synthesize augmented video sequences. Through this pipeline, we achieve coverage of 55 effect categories while maintaining quality via: (1) automated style-consistency checks, and (2) manual validation of visual fidelity.

B.2 Dataset Visualization

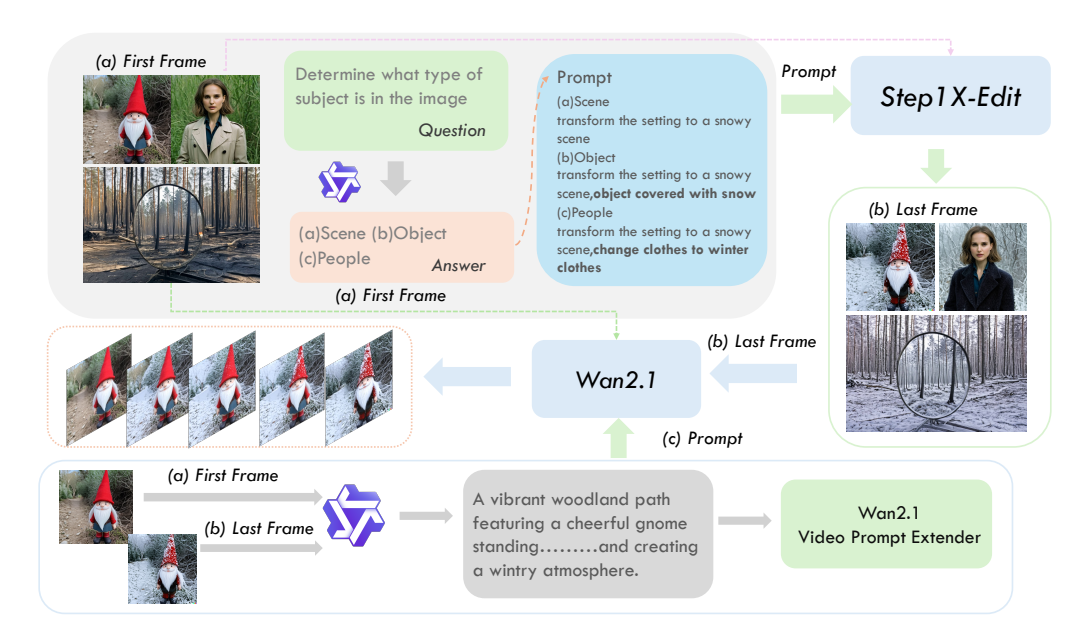


Figure 9: Synthetic VFX Video Generation via Keyframe Editing and WAN 2.1 Interpolation.

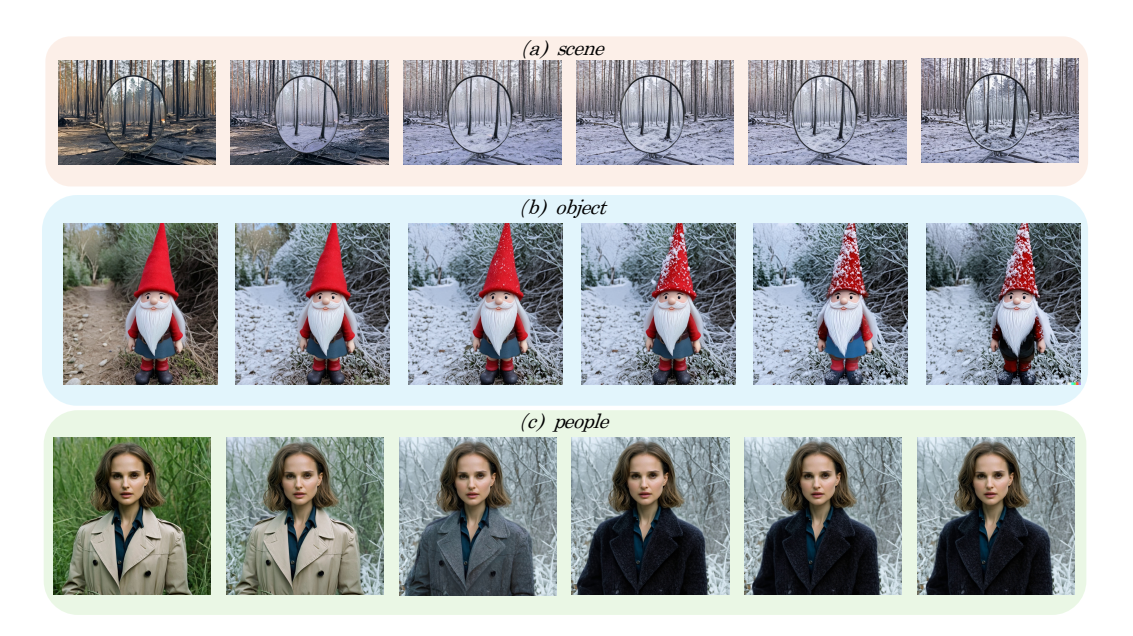


Figure 10: Some examples of our dataset curation pipeline.

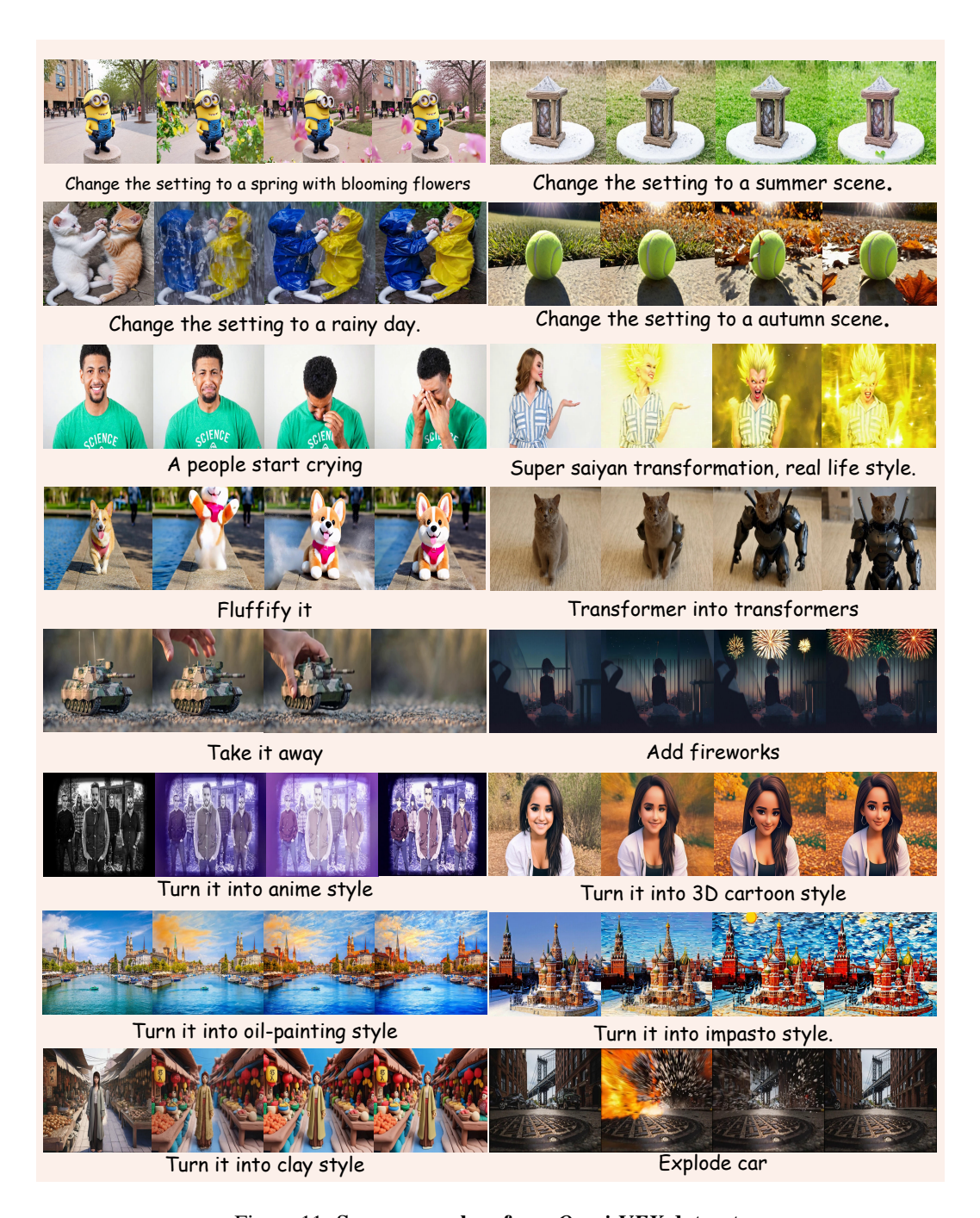


Figure 11: Some examples of our Omni-VFX dataset.

Our dataset consists of 55 diverse VFX samples, systematically categorized into five groups:

- Environmental Shifts: Including seasonal transitions (spring, summer, autumn, winter) and weather variations (e.g., rain).
- Dynamic Transformations: Featuring simulated phenomena such as explosions and fluid dynamics.
- 3. **Artistic Styles**: Comprising stylized renderings (e.g., oil painting effects, 3D doll aesthetics).
- Human Emotion Depictions: Capturing facial expressions (e.g., smiles, crying).
- Complex Effects: Integrating multiple visual elements across categories to produce sophisticated composites.

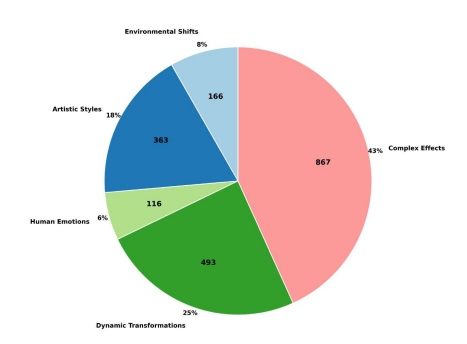


Figure 12: **Distribution of our** *Omni-VFX* **dataset.**

The representative visualizations are provided in Figure 11 while the distribution of samples across categories is illustrated in Figure 12.

C IMPLEMENTATION DETAILS

C.1 Training Data Augmentation

To address the scarcity of multi-VFX (Multiple Visual Effects) data, we perform data augmentation on single-VFX data. We sample single-VFX data along with their corresponding complete mask data with a probability of 20%; with a 40% probability, we sample single-VFX data and perform random cropping and splicing; and with a 40% probability, we sample two types of VFX and perform random cropping and splicing. During the splicing process, there is a 20% probability of applying temporal freezing to any segment of the spliced video (turning it into a static video with the corresponding mask set to empty, simulating the condition where no VFX is generated). The example of data augmentation is shown in Figure 13.

C.2 Non-Uniform Timestep Sampling

Through experiments, we observe that for video generation with strict control requirements, the denoising steps in the early stages of the diffusion model play a critical role, as they determine whether the target region achieves precise control. Traditional uniform timestep sampling requires extensive training to sufficiently optimize the model's accuracy in the initial steps. To accelerate training convergence, we enhance the focus on early denoising by allocating 3/4 of the batch to the crucial initial steps ([900, 1000]), while dedicating the remaining 1/4 to refining details in later steps ([0, 900]).

Tephoto if The in the interview of the i

Figure 13: Visualization of Data augmentation.

C.3 DUAL-PHASE TRAINING STRATEGY

To enhance the model's capability in controlling both single-VFX and multi-VFX videos' generation, we adopt a dual-stage progressive training strategy during the training phase:

- Stage 1: We train the model using single-VFX videos with single masks, allowing it to learn how to control a single VFX. This stage runs for 2,000 steps.
- Stage 2: In addition to single-VFX videos, we introduce multi-VFX videos by combining two VFXs (as described in Sec. C.1) and perform data augmentation on these samples. The model is fine-tuned for an additional 3,000 steps under this setting.

This training approach improves the model's robustness and enables it to generalize to a larger number of control VFXs (N > 2) during inference.

D METRICS

With the development of diffusion-based generative models Chu et al. (2025); Lan et al. (2025); Xu et al. (2025a), a series of evaluation benchmarks have emerged to assess the quality of generated content Ling et al.

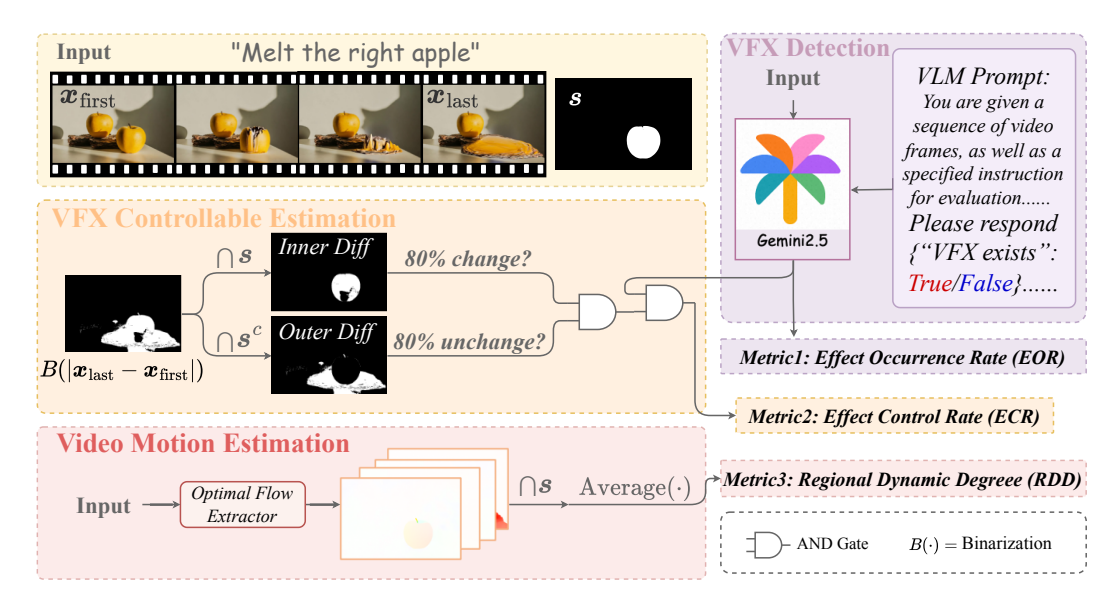


Figure 14: Flowchart of the metric design for controllable visual effect.

(2025); Feng et al. (2025); Chen et al. (2025); Huang et al. (2024a). However, existing benchmarks struggle to meet the evaluation requirements for controllable VFX.

Therefore, we propose an evaluation framework comprising three components: VFX detection, VFX controllable estimation, and video motion estimation, with the specific architecture illustrated in the Figure 14. These components correspond to the calculation processes of the metrics *Effect Occurrence Rate (EOR)*, *Effect Controllability Rate (ECR)*, and *Regional Dynamic Degree (RDD)*.

D.1 VISUAL EFFECTS DETECTION

To determine whether the desired visual effect is present in the generated videos, we leverage the Gemini 2.5 Comanici et al. (2025) large multimodal model as an evaluation assistant. Specifically, for each test video, we pair it with a predefined prompt template that explicitly describes the target effect, and input both into Gemini. We then request Gemini to provide a binary answer as to whether the specified effect has appeared in the video. Each query is repeated three times, and the most frequently occurring answer among the three is selected as the final result.

By applying this process to all videos in the evaluation set, we compute the *Effect Occurrence Rate (EOR)*, defined as the percentage of videos in which Gemini confirms the occurrence of the designated visual effect.

D.2 VISUAL EFFECTS CONTROLLABILITY ESTIMATION

Controllability estimation is performed only on videos that are identified as having the target effect by the Visual Effects Detection step. For these videos, we compute the absolute pixel-wise difference between the first and last frames and compute the resulting difference binary map. In the masked region, we select the top 80% of difference values; for the non-masked region, the bottom 80%. The mean squared error (MSE) is then computed as *Inner Diff* and *Outer Diff*. An effect is regarded as controllable if *Inner Diff* is below a threshold of 0.5 and *Outer Diff* is below a threshold of 0.1. The *Effect Controllability Rate (ECR)* is defined as the fraction of detected-effect videos that meet these criteria.

D.3 VIDEO MOTION DETECTION

The Regional Dynamic Degree (RDD) measures the strength of motion caused by VFX within mask-specified region of a video. We use the RAFT algorithm Teed and Deng (2020) to estimate optical flow between consecutive frames. Given a binary mask s for the region of interest, we calculate the mean motion magnitude within this region as follows:

$$RDD = \frac{1}{N} \sum_{t=1}^{N} \frac{1}{|\mathbf{s}|} \sum_{(x,y) \in \mathbf{s}} \|Flow(I_t, I_{t+1})_{x,y}\|_2,$$
(11)

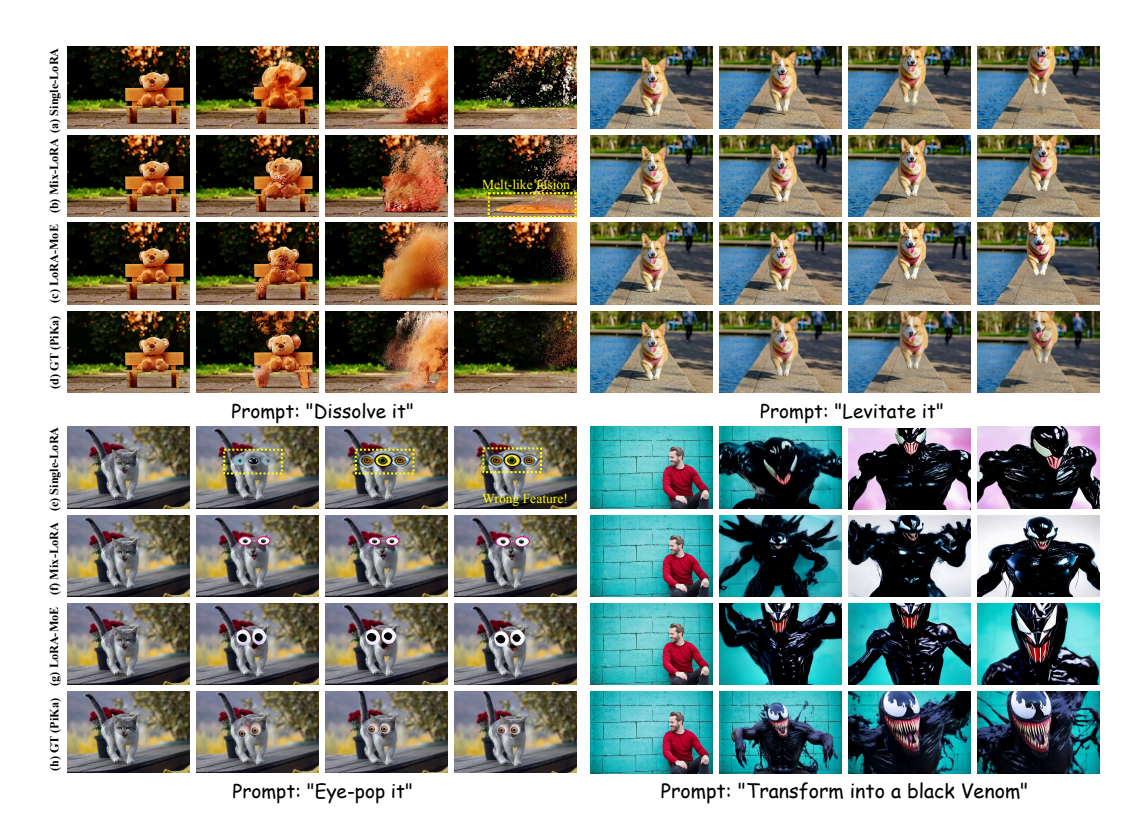


Figure 16: Qualitative Comparison of Different LoRA Settings.

where N is the number of consecutive frame pairs and |s| is the number of pixels in the masked region. A higher RDD indicates stronger or more dynamic effects within the specified area, enabling precise, region-specific evaluation of effect intensity.

E EXPERIMENTS RESULTS DETAILS

E.1 QUALITATIVE RESULTS OF LORA MOE

Qualitative results of Different LoRA settings are visualized in Figure 16. LoRA-MoE demonstrates superior visual performance.

E.2 QUALITATIVE RESULTS OF SINGLE-VFX CONTROL

Qualitative results of single-VFX control are visualized in Figure 15. CogV+CN incorrectly causes both cups to explode, while our proposed *Omni-Effects* explodes the correct cup while keeping the other cup intact.

E.3 USER STUDY OF MULTI-VFX GENERATION

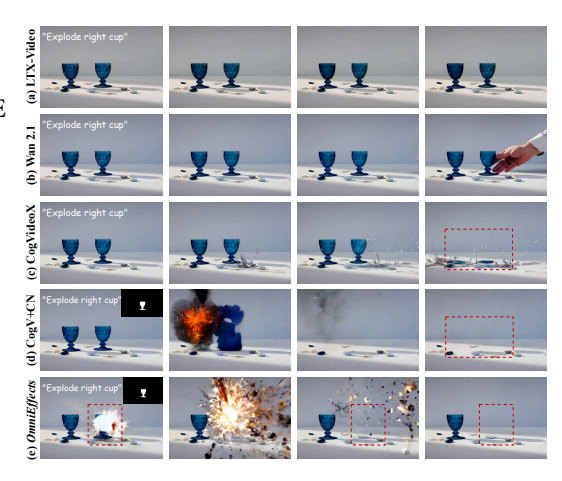


Figure 15: **Qualitative Comparison of Single-VFX Generation.** The desired outcome requires the right cup to explode while the left stays static.

To achieve more reliable evaluation results, we select a subset of videos from the test set for a user study. We choose the state-of-the-art open-source Wan2.1-I2V model as the representative base model, and evaluate it alongside **CogV+CN** and our proposed method on multi-effect videos. We design two questions: one regarding user preference (i.e., which video the user considers to be of the highest overall quality?), and another asking whether each video demonstrates precise controllability of the specified visual effect, which can directly reflect the effectiveness of our approach. Six professional raters participated in the evaluation, and the results are shown in Figure 17

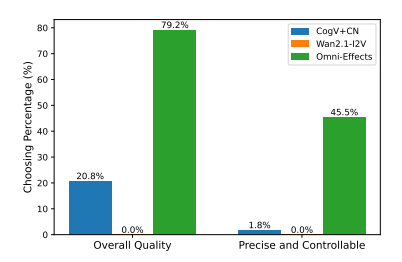


Figure 17: **User Study for Multi-VFX Generation.** *Omni-Effects* exceeds other baseline.

	Method	VFX Nums	Deflate	Melt	Crumble	Dissolve	Ta-da	Squish	Crush	Cake-ify
		1	913	2827	2947	1770	1053	1415	1496	2138
		2	857	3606	-	-	-	-	-	-
FVD↓	LoRA	4	779	3957	2324	1559	-	-	-	-
r ν D↓	LOKA	8	787	3456	2756	2103	1206	1699	1540	1355
		14	949	2030	2718	1722	1501	<u>1527</u>	1570	1388
]	LoRA MoE	14	839	2512	1641	1118	1064	1561	1213	1506

Table 5: Ablation Study on Co-trained with Different VFX Number.

F MORE ABLATION STUDY

F.1 VFX-COMBINATION TRAINING

Ablation studies on diverse VFX-combination training regimes (Table 5 and Table 6) reveal inherent effect clustering, demonstrating that compatible VFX-combination training enhances single-VFX generation quality. The proposed LoRA-MoE framework effectively leverages this property to boost performance across all VFX types.



Figure 18: **Ablation study on Non-uniform Timestep Sampling Steps. NUS** stands for Non-Uniform Sampling, and **DA** stands for Data Augmentation. The training of first stage N=1 with epoch=70.



Figure 19: Ablation Study on Different Training Strategy.

F.2 DATA AUGMENTATION

Ablation study on data augmentation (Figure 18) reveals that models struggle to achieve spatial controllability using single-VFX data alone without augmentation. Our custom-designed data augmentation protocol enables effective controllability for both single- and multi-VFX generation.

	Deflate	Deflate+Melt	Deflate+Squish
FVD↓	913	857(\(\psi 6\%)	1611(† 76%)

Table 6: Ablation Study on Co-trained with Different VFX combination.

F.3 TIMESTEP SCHEDULER

Ablation study on different time schedulers (Figure 18) reveals that traditional uniform sampling necessitates extensive training efforts to sufficiently optimize model accuracy in initial steps, whereas our employed non-uniform timestep sampling empirically accelerates model convergence.

F.4 TRAINING STRATEGY

Ablation study on different training strategies (Figure 19) reveals that our employed Dual-phase Training Strategy effectively enhances model robustness for multi-VFX generation, with Stage 2 demonstrably mitigating interference artifacts compared to Stage 1.